

BaFe₂Se₃: a high T_C magnetic multiferroic with large ferrielectric polarization

Shuai Dong,¹ J.-M. Liu,² and Elbio Dagotto^{3,4}

¹Department of Physics, Southeast University, Nanjing 211189, China

²National Laboratory of Solid State Microstructure, Nanjing University, Nanjing 210093, China

³Department of Physics and Astronomy, University of Tennessee, Knoxville, Tennessee 37996, USA

⁴Materials Science and Technology Division, Oak Ridge National Laboratory, Oak Ridge, Tennessee 37831, USA

(Dated: October 13, 2014)

The iron-selenides are important because of their superconducting properties. Here, an unexpected phenomenon is predicted to occur in an iron-selenide compound with a quasi-one-dimensional ladder geometry: BaFe₂Se₃ should be a magnetic ferrielectric system, driven by its magnetic block order via exchange striction. A robust performance (high T_C and large polarization) is expected. Different from most multiferroics, BaFe₂Se₃ is ferrielectric, with a polarization that mostly cancels between ladders. However, its strong magnetostriction still produces a net polarization that is large ($\sim 0.1 \mu\text{C}/\text{cm}^2$) as compared with most magnetic multiferroics. Its fully ferroelectric state, with energy only slightly higher than the ferrielectric, has a giant improper polarization $\sim 2 - 3 \mu\text{C}/\text{cm}^2$.

PACS numbers: 75.50.Ee, 74.70.Xa, 75.85.+t

Introduction. Low critical temperatures (T_C 's) and weak ferroelectric (FE) polarizations (P 's) are two important drawbacks of current type-II multiferroics, where P 's are driven by magnetism [1]. For this reason, a considerable effort recently focused on the design of new magnetic multiferroics to improve on T_C and its associated FE P . A recently confirmed example involves the quadruple-perovskite manganite CaMn₇O₁₂, with relatively large P ($\sim 0.3 \mu\text{C}/\text{cm}^2$) and T_C (90 K) [2], triggered by a new multiferroic mechanism [3, 4].

Despite the conceptual differences between superconductivity and multiferroicity, the search for high T_C superconductors (SCs) can help the magnetoelectric (ME) community to develop multiferroics with even higher T_C 's. For example, Kimura *et al.* found that CuO (a material related to Cu-oxide SCs) is actually a high- T_C type-II multiferroic between 213-230 K [5]. Besides the cuprates, the iron-based pnictides and chalcogenides have been intensively studied since 2008 because of their superconducting properties [6]. However, to our knowledge the possibility of multiferroic behavior has not been investigated before in any of these systems.

In this Letter, the iron-selenide BaFe₂Se₃ is predicted to hide a robust multiferroic order. Until now, BaFe₂Se₃ has been investigated as a member of the Fe-based superconductors family with only a handful of efforts that focused on magnetism [7–12] and (unconfirmed) superconductivity. Our prediction instead provides a novel and unexpected perspective of BaFe₂Se₃, that potentially may extend the search for multiferroics beyond this compound into the chalcogenides/pnictides families with tetrahedral anion cages.

BaFe₂Se₃ forms an orthorhombic structure. Each unit cell has two iron ladders (labeled as A and B), built by edge-sharing FeSe₄ tetrahedra, as shown in Fig. 1(a-b). Long-range antiferromagnetic (AFM) order is established below 256 K [8]. Both neutron studies and first-principles

calculations reported an exotic block AFM order [8–11] [Fig. 1(b-c)]. The Hartree-Fock approximation to the five-orbital Hubbard model also confirmed the stability of the block AFM phase and revealed other competing phases, e.g. the Cx phase [Fig. 1(d)] [13].

Symmetry analysis. The block AFM order is particularly interesting because it breaks parity symmetry and displays exchange striction effects. Indeed, the iron displacements are prominent, as revealed by neutron studies [7–10]: the nearest-neighbor (NN) distances between Fe(\uparrow)-Fe(\uparrow) [or Fe(\downarrow)-Fe(\downarrow)] at 200 K become 2.593 Å, much shorter than the Fe(\uparrow)-Fe(\downarrow) distance 2.840 Å [8]. However, this exchange striction is not sufficient to induce FE P since it breaks parity but not space-inversion symmetry. Thus, although neutron studies reported exchange striction effects in iron ladders [7–10], ferroelectricity has not been searched for in these materials.

The Se-tetrahedra also break parity in each ladder since Fig. 1(b) shows that Se(5) is above the ladder's plane but the next Se(7) is below, and the distances of Se(5) and Se(7) to the iron ladder plane should be the same in magnitude and opposite sign ("antisymmetric"). However, the block AFM order introduces a fundamental modification in the symmetry. Now the blocks made of four Fe(\uparrow)'s [or four Fe(\downarrow)'s] are no longer identical to blocks made of two Fe(\uparrow)'s and two Fe(\downarrow)'s. Then, the Se(5) and Se(7) heights do not need to be antisymmetric anymore; their distances to the ladder planes can become different. The same mechanism works for the edge Se's, e.g. Se(1) and Se(11). As a consequence, the Se atomic positions *break* the space inversion symmetry, generating a local FE P pointing perpendicular to the iron ladders plane (almost along the a -axis). Previous neutron studies [8] could have observed this effect, but in those investigations the Se positions were not discussed since the focus was not multiferroicity. Similar exchange striction works in the E-type AFM manganites and in Ca₃CoMnO₆ al-

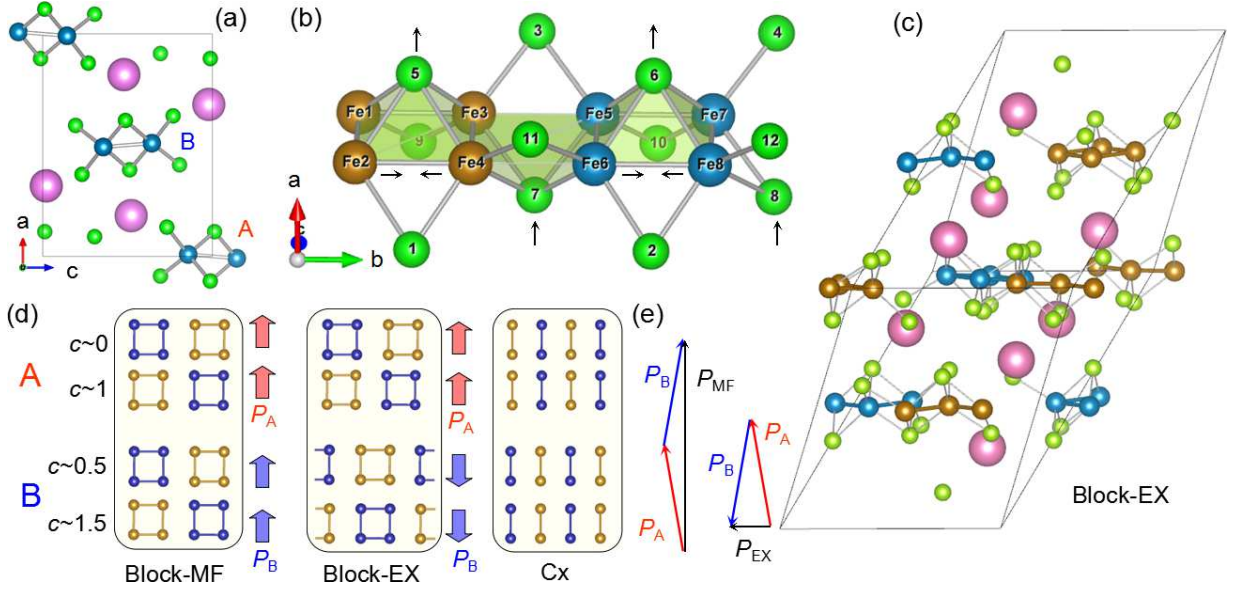


FIG. 1. (Color online) Crystal and magnetic structures of BaFe_2Se_3 . (a) Side view along the b -axis. Blue: Fe; green: Se; pink: Ba. (b) A Fe-Se ladder along the b -axis and its magnetic order. Partial ionic displacements driven by the exchange striction are marked as black arrows. (c) A unit cell considering the AFM magnetic order. (d) Spin structures. Left: Block-MF; middle: Block-EX; right: Cx. The side arrows denote the local FE P 's of each ladder. In (b-d), the spins (\uparrow/\downarrow) of Fe's are distinguished by colors. (e) Vector addition of FE P 's of ladders A and B.

though the details are not identical [14, 15].

Qualitatively, the ME coupling energy for each ladder [14] can be analytically expressed as:

$$F = \alpha(\mathbf{B}_1^2 - \mathbf{B}_2^2)P_{\perp} + \frac{1}{2\chi}\mathbf{P}^2, \quad (1)$$

with the parity order parameters $\mathbf{B}_1 = \mathbf{S}_1 + \mathbf{S}_2 + \mathbf{S}_3 + \mathbf{S}_4 - \mathbf{S}_5 - \mathbf{S}_6 - \mathbf{S}_7 - \mathbf{S}_8$; $\mathbf{B}_2 = \mathbf{S}_1 + \mathbf{S}_2 - \mathbf{S}_3 - \mathbf{S}_4 - \mathbf{S}_5 - \mathbf{S}_6 + \mathbf{S}_7 + \mathbf{S}_8$. \mathbf{S}_i denotes the spin of $\text{Fe}(i)$ as indicated in Fig. 1(b). α is the coefficient of exchange striction, proportional to $\frac{\partial J}{\partial r}$ where J and r are the exchange and distance between NN Fe's along the ladder direction, respectively. χ is the dielectric susceptibility of the paraelectric phase. P_{\perp} is the FE component perpendicular to the Fe ladder plane. By minimizing the energy, the induced P of each ladder can be obtained as $-\alpha\chi(\mathbf{B}_1^2 - \mathbf{B}_2^2)$, perpendicular to the ladder plane. This scheme is similar (but not identical) to that of E-type AFM $\alpha\text{-HoMnO}_3$ [14], and different in principle from geometric improper ferroelectrics [16].

This discussion suggests that each ladder can be multi-ferroic, but only the inclusion of inter-chain couplings can address if a macroscopic FE P will indeed be generated. According to neutron studies [8], the block AFM pattern shows a $\frac{\pi}{2}$ -phase shift between the NN A-B ladders but a π -phase shift between the NN A-A ladders (and NN B-B ladders), as in the Block-EX shown in Fig. 1(d). Then, the unit cell of BaFe_2Se_3 doubles when considering the magnetism [see Fig. 1(c)]. According to the analytical expression above, the π -shift between A-A ladders (or B-B ladders) will not change the direction of the induced

FE P [17] but the $\frac{\pi}{2}$ -phase shift between A-B ladders will induce (nearly) opposite FE P 's, as sketched in Fig. 1(d-e). A full cancellation does not occur due to a second key observation: a small canting angle exists between the ladders A and B planes [see Fig. 1(a)], leading to a residual FE P (P_{EX}) pointing almost along the c -axis [Fig. 1(e)]. The residual P_{EX} magnitude can be estimated by considering the tilting angle between the ladders A and B planes, which is about 5.4° according to experiments [8]. This small tilting gives $P_{\text{EX}} \approx 9.4\%P_A$.

Since the spin ladders in BaFe_2Se_3 are quasi-one-dimensional, the inter-ladder couplings should be weak compared to the intra-ladder couplings. Thus, it may be possible to overcome the $\frac{\pi}{2}$ -phase shift between ladders A and B by chemical substitution, or electric field. If this is achieved, the magnetic structure becomes the Block-MF state. In this case, the magnetism-induced FE P 's of all ladders will coherently produce a combined P_{MF} pointing along the a -axis [Fig. 1(e)], with an amplitude nearly twice that of P_A . All this intuitive analysis for the many possible magnetic states has been fully confirmed by formal group theory [18].

First-principles study. A density functional theory (DFT) calculation will be used to confirm above predictions [19]. The DFT results are in Fig. 2 varying the effective Hubbard interaction $U - J$, which give the following conclusions:

(1) Atomic positions were optimized with the relevant magnetic states [ferromagnetic (FM), Cx-type AFM, Block-MF, Block-EX, and non-magnetic (NM)], and

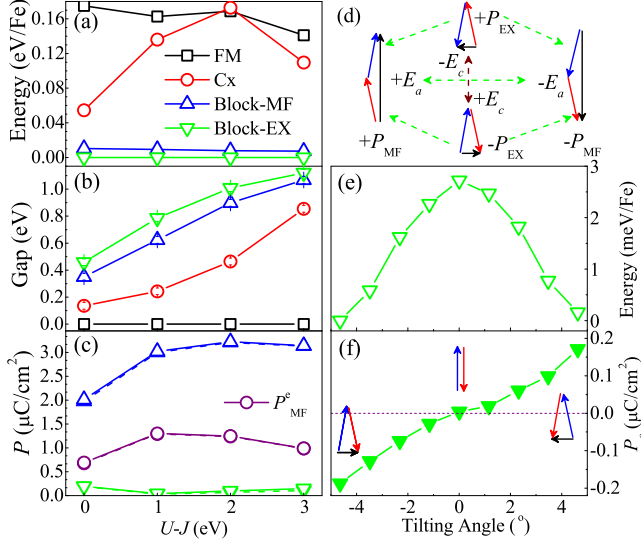


FIG. 2. (Color online) (a-c) DFT results varying the effective Hubbard interaction. (a) Energies for various magnetic states, with the Block-EX as reference. (b) Band gaps. NM and FM are metallic (zero gap). (c) The FE P 's of Block-MF and Block-EX states. The dashed lines (with solid symbols) are the components along the symmetry expected directions (e.g. a axis for Block-MF, c axis for Block-EX), which are almost identical to the total P and imply a successful prediction by the symmetry analysis. The purple P_{MF}^e 's (solid and open symbols) are the pure electronic contribution in the Block-MF case. (d) Sketch of switchings between $\pm P_{EX}$ and $\pm P_{MF}$ driven by the electric field E_x along the x ($x=a$ or c) direction. (e-f) DFT demonstration (without U) of switching between $\pm P_{EX}$ via the rotation of Fe-ladder planes. Horizontal axis: the angle between ladders A's and B's planes. The two limits ($\sim \pm 4.6^\circ$) denote the relaxed $\pm P_{EX}$ states, respectively. The center 0° denotes the relaxed non-tilting case. For other angles, the structures are obtained by proportional mixing among these three limits. Vertical axes: (e) energy per Fe; (f) polarization along the c -axis.

their energies were compared. As shown in Fig. 2(a), the Block-EX state is the lowest in energy, as in experiments [7–10]. The Block-MF is only slightly higher (7–10 meV/Fe). All other states are much higher. In the Block-EX state, the DFT NN Fe-Fe distance for Fe(\uparrow)-Fe(\uparrow) [or Fe(\downarrow)-Fe(\downarrow)] is ~ 2.584 Å and for Fe(\uparrow)-Fe(\downarrow) ~ 2.823 Å (without U), very similar to the neutron results mentioned before. More importantly, DFT finds that the heights of Se(5) and Se(7) are different: 1.64 Å and 1.42 Å (without U), respectively. This numerically confirms that the relaxed structures of the individual ladders do have a net electric moment.

(2) The density of states (DOS) were calculated to extract the energy gap around the Fermi level. As shown in Fig. 2(b), the FM and NM states are metallic while all other magnetic states are insulating. Note that the Block-EX energy gap is 0.46 eV without U , in agreement with previous DFT results (0.44 eV [10]) but much higher

than the value estimated from the resistance-temperature curves which is ~ 0.13 – 0.178 eV [9, 12]. This difference is important and will be further discussed below.

(3) The most important physical property is the FE P . The insulating and space-inversion symmetric Cx phase is considered as the nonpolar reference state. Confirming the previous symmetry analysis, both the Block-EX and Block-MF are found to be multiferroic in our DFT calculations. P_{MF} is large and mostly along the a -axis ($2.01 \mu\text{C}/\text{cm}^2$ without U and increases to $3.02 - 3.22 \mu\text{C}/\text{cm}^2$ with U). This value of P_{MF} is among the largest reported in type-II multiferroics, comparable with the E-type AFM manganites [14, 25, 26]. As discussed before, the Block-EX should be ferrielectric with a weaker P . This is also confirmed in our DFT calculation: the net FE P is mostly along the c -axis and its amplitude is $0.19 \mu\text{C}/\text{cm}^2$ without U , which is one order of magnitude smaller than P_{MF} as expected from the above symmetry analysis, and comparable with RMnO_3 ($R = \text{Tb}$ or Dy) [27]. The U -dependent P_{EX} is non-monotonic [19]. The DFT directions of P_{EX} and P_{MF} agree perfectly with the symmetry analysis, and the values of P_{EX} and P_{MF} are also in qualitative agreement.

(4) Although the experimental-measurable quantity is the total P , it is physically meaningful to analyze the individual contributions from ionic and electronic displacements. Previous DFT studies on type-II multiferroics reported that the electronic contribution could be significant [3, 25], contrary to proper ferroelectrics where the ionic displacements are always dominant. Thus, it is interesting to disentangle the electronic P^e and ionic P^{ion} contributions in BaFe_2Se_3 . To unveil the intrinsic physics of each ladder and avoid compensation effects between ladders, here the Block-MF case is analyzed. By adopting the relaxed structure with the Cx magnetic order and imposing the Block-MF spin order, the pure electronic contribution P_{MF}^e can be estimated: it results to be large (~ 0.69 – $1.3 \mu\text{C}/\text{cm}^2$, about $1/3$ of P_{MF} and parallel to P_{MF}).

(5) As sketched in Fig. 1(d), by shifting the magnetic blocks by one lattice constant in all ladders, both P_A and P_B are reversed according to the analytical formula above. Then both P_{EX} and P_{MF} can be flipped by 180° . The energies before and after such a 180° flipping are degenerate. As sketched in Fig. 2(d), to realize the flipping of P_{EX} , an external electric field should be applied along the c -axis. If a large enough field is applied along the a -axis, the ferrielectric (Block-EX) to FE (Block-MF) phase transition will occur, producing a 90° flipping and enhancement of P . Moreover, the 180° flipping of P_{EX} can also be obtained by reversing the tilting angle between the planes of ladders A-B, without shifting the magnetic blocks. As shown in Fig. 2(e), The calculated energy shows an almost symmetric barrier between the $+P_{EX}$ and $-P_{EX}$ states, with the height of the barrier of ~ 2.8 meV/Fe. Comparing with other FE materials, e.g.

8 meV/Mn for *o*-HoMnO₃ and 18 meV/Ti for BaTiO₃ [25], the required electric fields $\pm E_c$ should be accessible. Note that this switching path is an energetically “upper bound”, not necessarily the actual path occurring in experiments during switching, which may display an even lower energy barrier. In addition, a magnetic field can suppress the AFM order and its FE *P*, as in other spin- $\uparrow\uparrow\downarrow\downarrow$ multiferroics (e.g. Ca₃CoMnO₆ [15]), rendering an intrinsic ME coupling.

In summary, our DFT calculations fully confirm the proposed magnetic-induced ferrielectricity of BaFe₂Se₃. The multiferroic properties of BaFe₂Se₃ are very prominent: (1) high T_C close to room temperature; (2) large polarization in the ground state and even larger in the excitation state. Both these two properties are in the top-most range among all type-II multiferroics, i.e. BaFe₂Se₃ can be a quite interesting material.

Additional discussion. Since pure DFT always underestimates the band gap, the real band gap of BaFe₂Se₃ should be even larger, and the observed small gaps (0.13-0.178 eV [9, 12]) in transport may be caused by in-gap levels induced by impurities. In fact, non-stoichiometry and impurities are ubiquitous in all samples of BaFe₂Se₃ in previous experiments [8–10, 12], making these samples too conductive to detect ferro- or ferri-electricity.

To guide future experimental efforts, here results for the iron-selenides BaFe₂S₃ and KFe₂Se₃ are also presented. Although BaFe₂S₃ is very similar to BaFe₂Se₃, its space group is the orthorhombic *Cmcm* [28], identical to that of KFe₂Se₃ [8]. Furthermore, our DFT calculation on BaFe₂S₃ predicts a Cx ground state as found in KFe₂Se₃, in agreement with recent experiments [29]. Considering the magnetic similarity between BaFe₂S₃ and KFe₂Se₃, it is reasonable to assume that the Fe-Se bond in the latter may not be fully electrovalent due to the weak electronegativity of Se. In this sense, the real Fe valence in BaFe₂Se₃ is $1 + \delta$ (with δ between 0 and 1) instead of the nominal +2, which may be the reason for the experimental difficult to prepare pure BaFe₂Se₃ due to the instability of Fe^{(1+ δ)+}, which will induce iron vacancies [10]. Even the exotic AFM block state, with tetramer magnetic units, may be also caused by this $1 + \delta$ effect according to the mechanism of Peierls-like transition in one-dimensional lattices, e.g. at $\delta = \frac{3}{4}$ or $\delta = \frac{1}{4}$.

The argument above is clear in our DFT calculation. The electron density differences between BaFe₂Se₃ and BaFe₂S₃ are displayed in Fig. 3. The bright red spheres provide clear evidence that the S anions attract more electrons than Se. Meanwhile, the Fe cations lose more 3*d* electrons in BaFe₂S₃, characterized by bright blue lobes pointing along the Fe-S/Se directions. By contrast, the density difference is weak but also exists in the Fe-Fe ladder plane. Besides these two clear differences, outside the bright green spheres, there is a dim blue sphere surrounding each S/Se site, with negative value: this suggests that the outmost electrons of Se (S) are more extended (local-

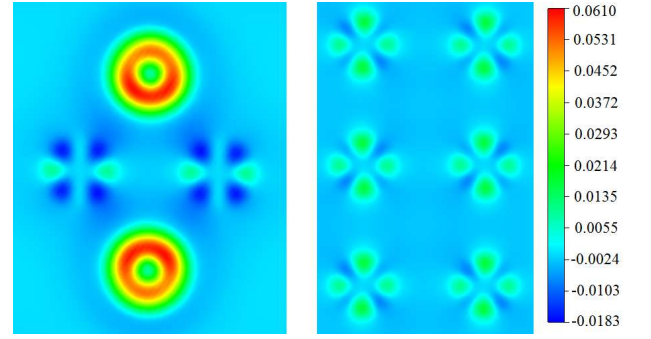


FIG. 3. (Color online) Two-dimensional profiles of electronic density difference (BaFe₂S₃ minus BaFe₂Se₃). Left: the Se(5)-Fe(3)-Fe(4)-Se(7) plane. Spheres denote the Se/S sites while multi-lobe ones the Fe sites. Right: the Fe-ladder plane.

ized), also supporting the covalent scenario for BaFe₂Se₃.

The analysis presented above reminds us of another iron-selenide, layered KFe₂Se₂, in which the nominal valence of Fe is +1.5 and a two-dimensional block AFM order exists in each layer [30]. According to the symmetry analysis, each layer of KFe₂Se₂ should be FE polarized due to the exchange striction. However, the FE *P* cancels between layers, resulting in an antiferroelectric material.

Prospect. It is recognized that electron correlations are crucial for high- T_C SCs, but they are also equally important in magnetic multiferroics, e.g. to stabilize the 2×2 spin block order of BaFe₂Se₃ [13] that eventually leads to the ferroelectricity discussed here. In fact, the parent materials of high- T_C SCs and type-II multiferroics are both antiferromagnets with full or partial Motttness. More in general, the consequences of correlation such as the orbital-selective Motttness [31], frustrating effects in magnetism, and even strong electron-phonon couplings [32], all may provide a common fertile environment for both superconductivity and multiferroicity to develop. While it is still an open question to show convincingly whether this leads to cooperation or competition between the two states, BaFe₂Se₃ establishes a good starting point to explore these ideas.

Summary. Using a symmetry analysis and first-principles calculations, the multiferroicity of BaFe₂Se₃ has been predicted. Different from most previous magnetic multiferroics, BaFe₂Se₃ should be ferrielectric but its net polarization remains large and its critical temperature high. Its corresponding ferroelectric phase (close in energy) has a giant polarization. The multiferroic performance of BaFe₂Se₃ is in the topmost range in the type-II multiferroic family, making it an attractive system for further studies. The present experimental difficulty to obtain a pure phase is here explained by the covalent bonds scenario. Our study broadens the research area of multiferroics and leads to a cross fertilization between superconductors and multiferroics.

We thank K.F. Wang, P. Yu, L. Li, M.F. Liu, J. Neilson, S.-W. Cheong, H.J. Xiang, Q.F. Zhang, Q. Luo, C.L. Zhang, and H. Takahashi for helpful discussions. Work was supported by the 973 Projects of China (2011CB922101) and NSFC (11274060, 51322206, 11234005). E.D. was supported by the U.S. DOE, Office of Basic Energy Sciences, Materials Sciences and Engineering Division.

-
- [1] D. Khomskii, *Physics* **2**, 20 (2009); S.-W. Cheong and M. Mostovoy, *Nat. Mater.* **6**, 13 (2007); K. F. Wang, J.-M. Liu, and Z. F. Ren, *Adv. Phys.* **58**, 321 (2009); S. Dong and J.-M. Liu, *Mod. Phys. Lett. B* **26**, 1230004 (2012).
 - [2] G. Q. Zhang, S. Dong, Z. B. Yan, Y. Y. Guo, Q. F. Zhang, S. Yunoki, E. Dagotto, and J.-M. Liu, *Phys. Rev. B* **84**, 174413 (2011); R. D. Johnson, L. C. Chapon, D. D. Khalyavin, P. Manuel, P. G. Radaelli, and C. Martin, *Phys. Rev. Lett.* **108**, 067201 (2012).
 - [3] X. Z. Lu, M.-H. Whangbo, S. Dong, X. G. Gong, and H. J. Xiang, *Phys. Rev. Lett.* **108**, 187204 (2012).
 - [4] S. Dong, R. Yu, J.-M. Liu, and E. Dagotto, *Phys. Rev. Lett.* **103**, 107204 (2009); N. J. Perks, R. D. Johnson, C. Martin, L. C. Chapon, and P. G. Radaelli, *Nat. Commun.* **3**, 1277 (2012); M. Mostovoy, *Physics* **5**, 16 (2012).
 - [5] T. Kimura, Y. Sekio, H. Nakamura, T. Siegrist, and A. P. Ramirez, *Nat. Mater.* **7**, 291 (2008).
 - [6] D. C. Johnston, *Adv. Phys.* **59**, 803 (2010); G. R. Stewart, *Rev. Mod. Phys.* **83**, 1589 (2011); E. Dagotto, *ibid.* **85**, 849 (2013).
 - [7] A. Krzton-Maziopa, E. Pomjakushina, V. Pomjakushin, D. Sheptyakov, D. Chernyshov, V. Svitlyk, and K. Conder, *J. Phys.: Condens. Matter* **23**, 402201 (2011); V. Svitlyk, D. Chernyshov, E. Pomjakushina, A. Krzton-Maziopa, K. Conder, V. Pomjakushin, R. Pöttgen, and V. Dmitriev, *ibid.* **25**, 315403 (2013).
 - [8] J. M. Caron, J. R. Neilson, D. C. Miller, A. Llobet, and T. M. McQueen, *Phys. Rev. B* **84**, 180409(R) (2011); J. M. Caron, J. R. Neilson, D. C. Miller, K. Arpino, A. Llobet, and T. M. McQueen, *ibid.* **85**, 180405(R) (2012).
 - [9] Y. Nambu, K. Ohgushi, S. Suzuki, F. Du, M. Avdeev, Y. Uwatoko, K. Munakata, H. Fukazawa, S. Chi, Y. Ueda, and T. J. Sato, *Phys. Rev. B* **85**, 064413 (2012).
 - [10] B. Saparov, S. Calder, B. Sipos, H. Cao, S. Chi, D. J. Singh, A. D. Christianson, M. D. Lumsden, and A. S. Sefat, *Phys. Rev. B* **84**, 245132 (2011).
 - [11] M. V. Medvedev, I. A. Nekrasov, and M. V. Sadovskii, *JETP Lett.* **95**, 37 (2012).
 - [12] H. Lei, H. Ryu, A. I. Frenkel, and C. Petrovic, *Phys. Rev. B* **84**, 214511 (2011).
 - [13] Q. Luo, A. Nicholson, J. Rincón, S. Liang, J. Riera, G. Alvarez, L. Wang, W. Ku, G. D. Samolyuk, A. Moreo, and E. Dagotto, *Phys. Rev. B* **87**, 024404 (2013).
 - [14] I. A. Sergienko, C. Şen, and E. Dagotto, *Phys. Rev. Lett.* **97**, 227204 (2006).
 - [15] Y. J. Choi, H. T. Yi, S. Lee, Q. Huang, V. Kiryukhin, and S.-W. Cheong, *Phys. Rev. Lett.* **100**, 047601 (2008).
 - [16] E. Bousquet, M. Dawber, N. Stucki, C. Lichtensteiger, P. Hermet, S. Gariglio, J.-M. Triscone, and P. Ghosez, *Nature (London)* **452**, 732 (2008); N. A. Benedek and C. J. Fennie, *Phys. Rev. Lett.* **106**, 107204 (2011); Y. Yang, J. Íñiguez, A.-J. Mao, and L. Bellaiche, *ibid.* **112**, 057202 (2014).
 - [17] Note that all the ladders, either A or B, have the same staggered pattern of Se atoms above and below the ladder planes, i.e. a plaquette with a Se(5) above the ladder plane for ladder A, corresponds to another Se(5) above the ladder plane for ladder B, for the same plaquette.
 - [18] Using the experimental structure (space group No. 62, *Pnma*, orthorhombic) plus the particular magnetic order, the magnetic space group becomes monoclinic: (1) No. 14, *P21/c* for the Cx phase; (2) No. 9, *Cc* for the Block-EX phase; (3) No. 8, *Cm* for the Block-MF phase. The point group of *P21/c* is *2/m* which is a nonpolar point group. Then, *P* is forbidden in this group. The point group of both *Cc* and *Cm* is *m*, which is a polar point group and allows *P*.
 - [19] See Supplemental Material, which includes Refs. [20-24].
 - [20] P. E. Blöchl, O. Jepsen, and O. K. Andersen, *Phys. Rev. B* **49**, 16223 (1994).
 - [21] G. Kresse and J. Hafner, *Phys. Rev. B* **47**, 558 (1993).
 - [22] G. Kresse and J. Furthmüller, *Phys. Rev. B* **54**, 11169 (1996).
 - [23] S. L. Dudarev, G. A. Botton, S. Y. Savrasov, C. J. Humphreys, and A. P. Sutton, *Phys. Rev. B* **57**, 1505 (1998).
 - [24] R. D. King-Smith and D. Vanderbilt, *Phys. Rev. B* **47**, 1651 (1993).
 - [25] S. Picozzi, K. Yamauchi, B. Sanyal, I. A. Sergienko, and E. Dagotto, *Phys. Rev. Lett.* **99**, 227201 (2007).
 - [26] M. Nakamura, Y. Tokunaga, M. Kawasaki, and Y. Tokura, *Appl. Phys. Lett.* **98**, 082902 (2011).
 - [27] T. Kimura, G. Lawes, T. Goto, Y. Tokura, and A. P. Ramirez, *Phys. Rev. B* **71**, 224425 (2005).
 - [28] H. Y. Hong and H. Steinfink, *J. Solid State Chem.* **5**, 93 (1972).
 - [29] H. Takahashi, private communication.
 - [30] W. Li, S. Dong, C. Fang, and J. P. Hu, *Phys. Rev. B* **85**, 100407(R) (2012); W. Li, H. Ding, Z. Li, P. Deng, K. Chang, K. He, S. Ji, L. Wang, X. Ma, J.-P. Hu, X. Chen, and Q.-K. Xue, *Phys. Rev. Lett.* **109**, 057003 (2012).
 - [31] L. de' Medici, G. Giovannetti, and M. Capone, *Phys. Rev. Lett.* **112**, 177001 (2014).
 - [32] S. Liang, A. Moreo, and E. Dagotto, *Phys. Rev. Lett.* **111**, 047004 (2013).